Charged nanoparticle in a nanochannel: Competition between electrostatic and dielectrophoretic forces

Zachery K. Hulings, Dmitriy V. Melnikov, and Maria E. Gracheva

Phys. Rev. E **91**, 062713 — Published 18 June 2015

DOI: 10.1103/PhysRevE.91.062713

A charged nanoparticle in a nanochannel: Competition between electrostatic and dielectrophoretic forces

Zachery K. Hulings, Dmitriy V. Melnikov, and Maria E. Gracheva*
Department of Physics, Clarkson University, Potsdam, NY 13699

Nanochannels made in solid-state materials are used for various applications such as nanoparticle separation or DNA manipulation. In this work we examine the effects of the electric and dielectrophoretic forces on a charged nanoparticle confined in a nanochannel. To this end, we solve the Poisson equation for the nanochannel with a wedge-like geometry, and consider how channel geometry and electrolyte concentration affect the electrostatic potential distribution and forces acting on nanoparticles of various sizes. On the basis of our calculations, we establish conditions necessary for particle's attraction to the corners of a channel. We find that for large particles, the net force is attractive only for low concentrations of the electrolyte irrespective of the wedge angle, while small enough particles are attracted to the vertex for either larger electrolyte concentrations or small wedge angle.

I. INTRODUCTION

Recently, the study of the dynamics of biomolecules confined inside nanofluidic devices, such as nanochannels, attracted considerable attention [1–5]. Much of the interest in these systems stems from the experimental observation that nanochannels can be used to manipulate molecules. In particular, the degree of DNA stretching has been studied extensively for different nanochannel sizes and geometries, as well as electrolyte concentrations. It has been shown that a DNA molecule inside a nanochannel will have larger extensions for smaller electrolyte concentrations or for a smaller cross section size of a nanochannel [1, 3, 6–10]. In addition, the length of a stretched DNA molecule affects its mobility, which suggests that nanochannels can be used for separating molecules by length [2, 11–13]. Nanochannels have also been suggested to be used for fast, cheap DNA sequencing with single nucleotide precision by a variety of techniques. For example, one technique measures the transverse tunneling current as the stretched out DNA translocates through the channel [14–16].

It has also been experimentally shown that when a DNA molecule moves through a silicon dioxide nanochannel, it is attracted to the side walls and corners of the device [1, 2, 5]. The mechanism of this attraction is not clearly understood because silicon dioxide has a negative surface charge density, and so does the DNA molecule, and as such, one would expect them to repel each other. There has been proposed two explanations for this phenomenon. According to Ref.[5], the attraction of nanoparticles to the sidewalls or corners of the nanochannel could be the result of the dielectrophoretic force overcoming the electrostatic repulsion. The same group performed experiments on a colloidal solution of nanoparticles rather than on complex DNA molecules in an attempt to identify the mechanism of attraction of nanoparticles to the nanochannel walls. The other possible explanation is the roughness of the surfaces of nanochannels, which acts like a "barrier" for particles near the surface, so that they may be temporarily trapped along the surface [2].

In order to better understand the origin for a nanoparticle attraction to the surface of the nanochannel, in this work numerical investigation of a charged particle dynamics inside a nanochannel are performed. We consider only one particle interacting with the channel walls, thus assuming a dilute solution. We first compute the electrostatic potential in the vicinity the corner of a nanochannel by solving Poisson equation within the Debye approximation. From the potential, we calculate the electric field, and both the electrostatic the dielectrophoretic forces induced on a single, charged, spherical nanoparticle of a dilute species. We then examine the resulting nanoparticle dynamics for various geometries of a nanochannel, particle sizes, and electrolyte concentrations.

The paper is organized as follows. In Section II, after the description of our nanochannel geometry, the details on the solution of the Poisson equation and the dielectrophoretic force calculations are presented. In Section III, the analysis of our results is given, while Section IV contains a brief summary of our work.

II. MODEL

In our calculations we assume that the nanochannel is very long, so that we can disregard effects associated with its ends. As such, the problem becomes two-dimensional. A two dimensional cross section of the region near a corner of a nanochannel which we model as a wedge-like structure is shown in Fig. 1, with the angle between the two sides represented as α. The two sides of the wedge (the side walls of our nanochannel) have a constant surface charge density of $\sigma_s = -0.08$ e/nm^2, and electrolyte solution (KCl) is present everywhere inside the channel [17].

[1] *Corresponding author: gracheva@clarkson.edu

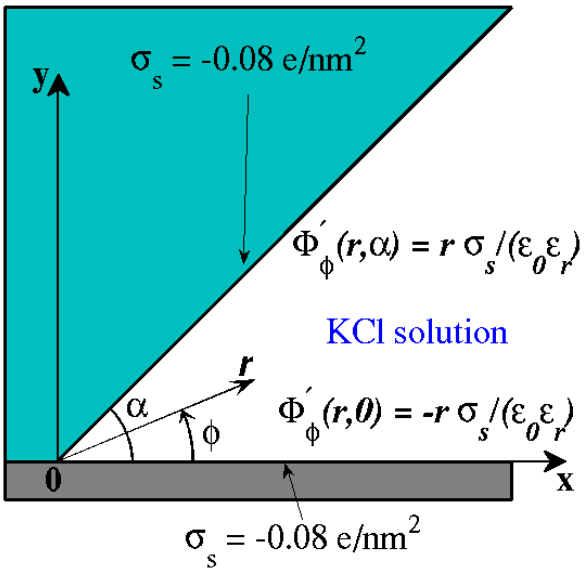

FIG. 1: (Color online) Schematics of the x-y cross section near a corner of a nanochannel which extends along the z-axis.

We first calculate the electrostatic potential inside the nanochannel. To do this, we solve Poisson equation in cylindrical coordinates in the Debye approximation:

$$\frac{1}{r}\frac{\partial}{\partial r}\left(r\frac{\partial \Phi}{\partial r}\right)+\frac{1}{r^2}\frac{\partial^2 \Phi}{\partial \phi^2}=\kappa^2\Phi, \tag{1}$$

where, $\kappa = L_D^{-1}$ is the inverse Debye screening length, $L_D = \left(\epsilon_0\epsilon_r k_B T/2Ce^2\right)^{1/2}$, $\epsilon_r = 78$ is the relative permittivity of the electrolyte solution, k_BT is the thermal energy with $T = 300$K, and C is the bulk electrolyte concentration.

The boundary conditions for solving Eq. (1) are set on the walls of the nanochannel:

$$\begin{aligned}\frac{\partial \Phi(r,0)}{\partial \phi} &= -\frac{r\sigma_s}{\epsilon_r\epsilon_0}\\ \frac{\partial \Phi(r,\alpha)}{\partial \phi} &= \frac{r\sigma_s}{\epsilon_r\epsilon_0}.\end{aligned} \tag{2}$$

They correspond to the case of the constant surface charge density (see Fig. 1).

Far from the vertex, normal to the surface of the channel, the electrostatic potential approaches that of a plane solution, with V_∞ being the potential value on the surface, which in the Debye approximation is equal to $V_\infty = \sigma_s L_D/\epsilon_0\epsilon_r$ [18]. Since the Debye approximation can be applied when $eV_\infty < 4k_BT$, the lowest limit of usable KCl concentrations in our work is 3 mM [19].

With help of the Kontorovich-Lebedev transform [20], the solution of Eq. (1) with boundary conditions (2) everywhere inside the channel can be written in the form [18, 21]:

$$\Phi(r,\phi) = \frac{2V_\infty}{\pi}\int_0^\infty \frac{\sinh\left[\frac{\lambda\pi}{2}\right]}{\sinh[\lambda\alpha]}\times \left(\cosh[\lambda\phi]+\cosh[\lambda(\phi-\alpha)]\right)K_{i\lambda}(\kappa r)d\lambda \tag{3}$$

where $K_{i\lambda}(\kappa r)$ is the modified Bessel function of the second kind of imaginary order [22] with λ being its order. To calculate the values of the electrostatic potential inside our nanochannel, numerical integration of Eq. (3) was performed (see Appendix for details).

In order to calculate the net force acting on the spherical charged particle in the electrolyte, in general, one has to compute the Maxwell stress tensor [23]. This requires full self-consistent calculation of the electrostatic potential for the nanochannel-particle system in the electrolyte solution. However, in order to get a clearer insight in the origin of the possible particle's attraction to the surface of the nanochannel, in this work we consider the total potential energy of the particle, U_{Total}, as the sum of the particle's electrostatic potential energy, U_p, and dielectrophoretic potential energy, U_d, i,e., we write

$$U_{Total} = U_p + U_d. \tag{4}$$

This approach works when the radius of the particle, R_p, is smaller than the characteristic length over which $\Phi(r,\phi)$ changes, i.e., $R_p \lesssim L_D$.

In the computation of U_p, we assume that the particle is charged with a surface charge density of $\sigma_p = -10^{-2}$ e/nm^2, which corresponds to that of a polystyrene latex sphere[24], so that

$$U_p = \sigma_p \oint \Phi da, \tag{5}$$

where the integral is taken over the particle's surface.

For a small particle with $R_p \lesssim L_D$, we can approximate the dielectrophoretic potential energy as [25]:

$$U_d = -2\pi R_p^3 \epsilon_r\epsilon_0 K|\nabla\Phi|^2, \tag{6}$$

where K is the static Clausius-Mossotti factor [26],

$$K = \frac{\varsigma_p - \varsigma_m}{\varsigma_p + 2\varsigma_m}, \tag{7}$$

with ς_p and ς_m being the static conductivities of the particle and the electrolyte solution, respectively [25]. From Eq. (7) one can see that for $\varsigma_p \gg \varsigma_m, K \simeq 1$, while for $\varsigma_p \ll \varsigma_m, K \simeq= -1/2$. Thus, depending on the ratios of the particle and solution conductivities, the dielectrophoretic force changes from repulsive to attractive or zero when $\varsigma_p = \varsigma_m$. As mentioned in Ref.[5] the static conductivity of a polystyrene bead is $\sim 10^{-2}$ S/m, which relative to the conductivity of a very low electrolyte solution, i.e., water, gives $K = 0.97$. However, in principle K can vary for particles of different sizes and materials

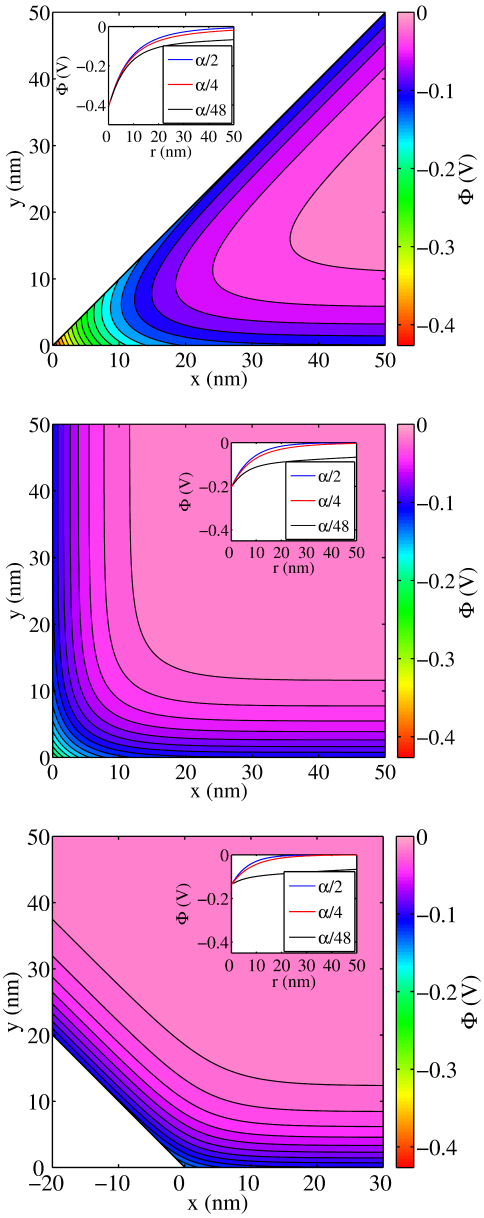

FIG. 2: (Color online) Contour plots of the electrostatic potential, $\Phi(r,\phi)$, inside the wedge for $\alpha = 45°$, $\alpha = 90°$, and $\alpha = 135°$, top to bottom, for $C = 3$ mM. The inset in each shows line plots of the electrostatic potential along certain angles.

relative to the medium. As such, we consider in this work $-1/2 \leq K \leq 1$.

In the limiting case of a small particle ($R_p \ll L_D$) interacting with a charged plane ($\alpha = 180°$ in Fig. 1), the electric and dielectrophoretic potential energies [Eqs. (5) and (6)], respectively, become

$$U_p(r) = QV_\infty e^{-\kappa r} \tag{8}$$

$$U_d(r) = -QV_\infty \frac{\sigma_s \kappa R_p K e^{-2\kappa r}}{2\sigma_p}, \tag{9}$$

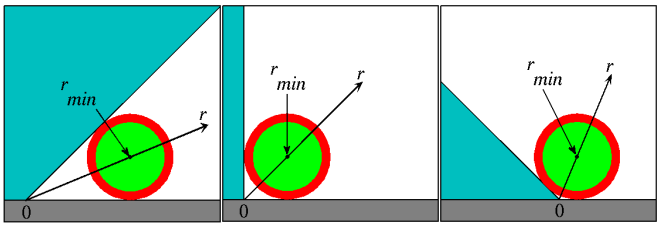

FIG. 3: (Color online) Schematic representation of a spherical particle located at its position closest to the vertex of a nanochannel for $\alpha = 45°$, $90°$, and $135°$, left to right. Each outer (red) ring has a thickness of 0.4 nm, and represents the thickness of the surface layer over which the charge is distributed.

TABLE I: Values of r_{min} and particle's net charge Q for different R_p and wedge angles α.

R_p (nm)	r_{min} (nm)				Q (e)
	$\alpha = 45°$	$\alpha = 90°$	$\alpha = 135°$	$\alpha = 180°$	
1.0	2.6	1.4	1.1	1	0.13
3.0	7.8	4.2	3.2	3	1.1
5.0	13	7	5.5	5	3.3

where r is the distance between the particle and the plane, and Q is the particle's charge.

III. RESULTS

We first consider how the value of the wedge angle α affects the electric potential $\Phi(r,\phi)$ near the corners of a nanochannel. In Fig. 2 we present contour plots of the electrostatic potential distributions for $\alpha = 45°$, $90°$ and $135°$ and electrolyte concentration $C = 3$ mM. The inset in each shows line plots of the electrostatic potential along certain angles ϕ. As one can see, the largest variation in the potential occurs near the vertex, which in general results in a stronger electric field and a larger dielectrophoretic potential in that region. One can also see from this figure that the smaller the wedge angle α, the larger the variation in the electrostatic potential near the vertex. Similar results (not shown) but with smaller values of $\Phi(r,\phi)$ were obtained for a concentration of 10 mM. Since the Debye length for $C = 10$ mM is ~ 3.0 nm and for $C = 3$ mM is ~ 5.6 nm, we limit ourselves to a particle with a maximum radius of 5 nm.

Next, we study the total potential, U_{Total}, acting on a dielectric particle, and investigate how different particle sizes, angles α, and values of constant K affect it. Due to their finite size, particles can never approach the origin, ($r \to 0$). Thus, we first compute how close it can get to the vertex ($x = y = 0$ in Fig. 2), i.e., the minimum distance between the vertex and the particle's center, r_{min}, measured along the bisecting line (see Fig. 3). The values of r_{min} together with corresponding total charge Q of the

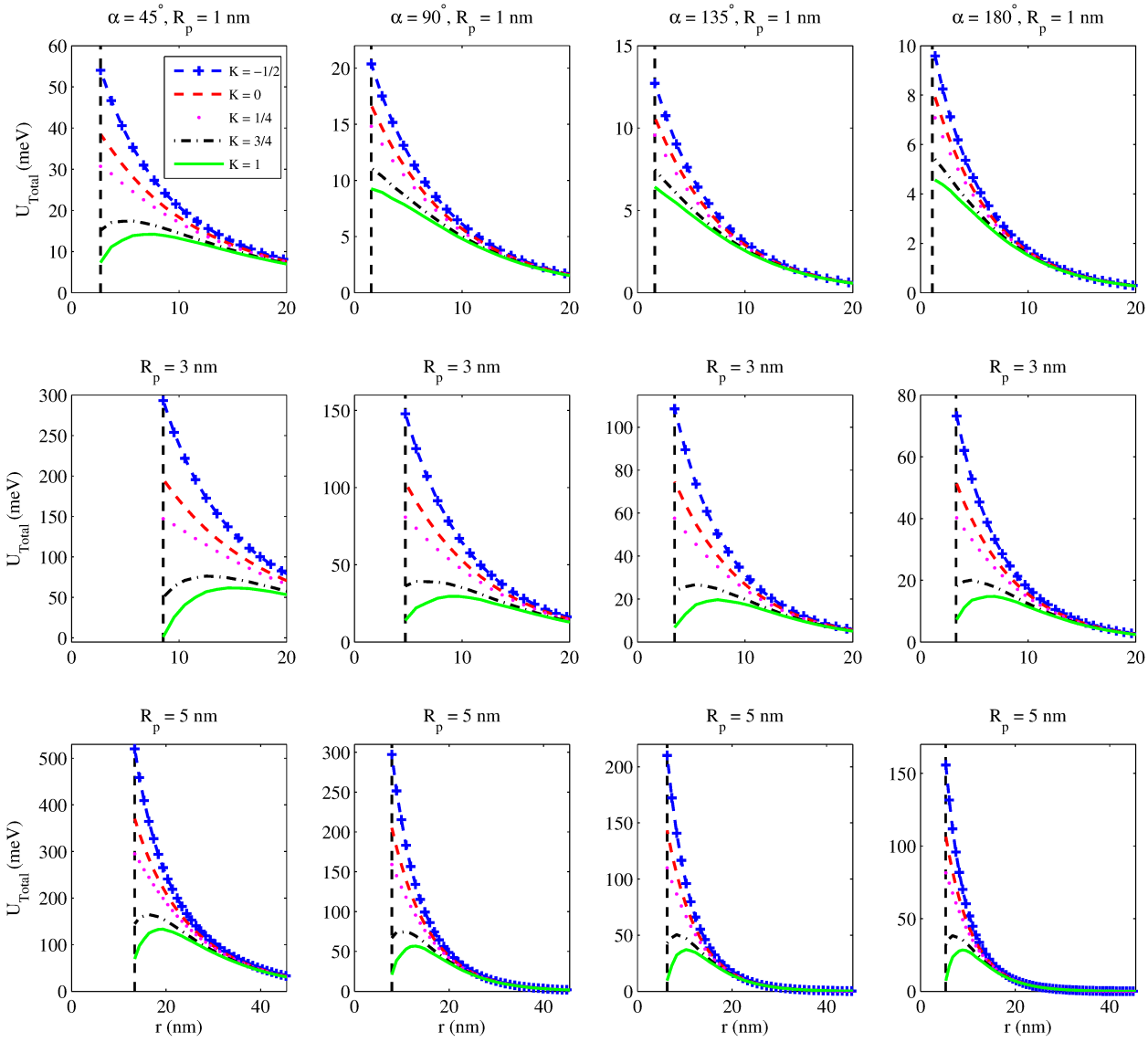

FIG. 4: (Color online) Total potential, U_{Total}, for different wedge angles, α with $C = 3$ mM, along the bisecting angle of the wedge for K = -1/2 (plus dashed blue line), 0 (dashed red line), 1/4 (pointed magenta line), 3/4 (dash dotted black line), and 1 (solid green line). The black dashed line shows the location of r_{min} value (see Table 1).

particle are summarized in Table 1 for different angles α and for different particle sizes.

Figures 4 and 5 show the total electric potential energy, U_{Total}, computed using Eqs. (3) - (6) along the bisecting angles for the same R_p and α as in Table 1, for $C = 3$ mM and 10 mM, respectively. The right most column in these figures ($\alpha = 180°$) corresponds to the case of a particle interacting with a charged plane.

Since a particle is attracted to the vertex when the slope of U_{Total} is positive, one can see from Figs. 4 and 5 that in general the strongest attraction force occurs when r is small. We also see that the particle is attracted to the vertex only when $K = 1$ or 3/4, with $K = 1$ clearly corresponding to the strongest attraction (largest positive slope of U_{Total} for small r), and with an attractive force extending further away from the vertex for all studied cases.

For $C = 3$ mM, Fig. 4, we see that a particle will be attracted to the vertex for all four studied angles α when its radius $R_p = 3$ and 5 nm, with a positive slope generally extending farther out from the vertex for the 5 nm particle. On the other hand, when $R_p = 1$ nm, only for $\alpha = 45°$ the particle is attracted to the vertex. The reason for that is that for small $R_p < L_D$ and $\alpha \to 180°$, the dielectrophoretic potential is much smaller than the Coulomb potential (near the surface of the channel the ratio $\frac{U_p}{U_d} \simeq 2\frac{\sigma_p}{\sigma_s}\frac{L_D}{R_p} > 1$, see Eqs. (8) and (9)), so that the small particles are repelled. However, when α decreases,

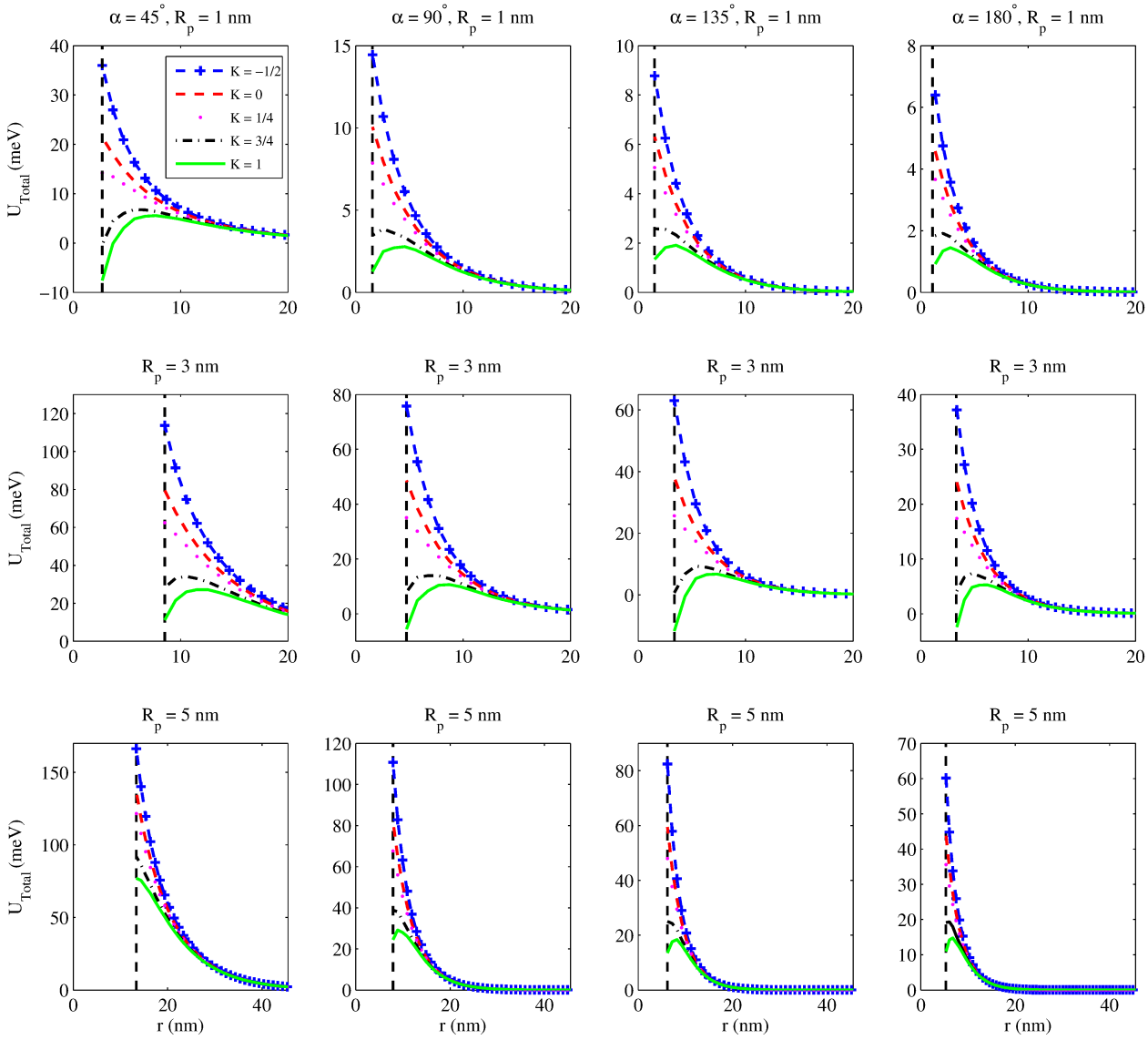

FIG. 5: (Color online) Same as in Fig. 4 but for $C = 10$ mM.

the potential varies more strongly, that is the magnitude of the electric field increases, see Fig. 2, and as a result, the attractive dielectrophoretic force increases and eventually overcomes the repulsive Coulomb force. For larger particles, $R_p > L_D$, this is manifested in the increasing range of the region in which a particle is attracted to the vertex. For comparison, the magnitudes of the attractive force acting on a particle at its closest position to the vertex for $K = 1$ and $\alpha = 45°$ is 0.61, 3.9, and 4.5 pN for $R_p = 1$, 3, and 5 nm, respectively. To show how U_{total} affects the distribution of particles near the vertex, we can use the Boltzmann distribution to calculate the ratio of particle densities at its closest position to the vertex to its farthest point on the plot. For the best case scenario at 3 mM solution concentration, we found that this ratio is ∼7.9 for $K = 1$, $\alpha = 45°$, and $R_p = 3$ nm, which indicates that particles are more likely to be found near the vertex.

In order to see how decreasing Debye length modifies the particle's behavior, in Fig. 5 we show the total potential energy, U_{Total}, computed for larger electrolyte concentration of 10 mM. Using the same analysis as for Fig. 4, we see that a particle can be attracted to the vertex for all four angles α both for $R_p = 1$ and 3 nm. On the other hand, when $R_p = 5$ nm, it is repelled for $\alpha = 45°$, while for other wedge angles there is a narrow range of distances from the vertex where the slope of U_{Total} is positive (the force is attractive). This can be attributed to a smaller Debye length leading to a faster decay of the dielectrophoretic force with the distance of the surface as compared to the Coulomb force, see Eqs. (8) and (9), so that large particles simply cannot get in the region of the

strong electric field near the vertex. Similarly to the case in Fig. 4, it can be seen that the region where the slope is of U_{Total} is positive extends further from the vertex for $R_p = 3$ nm and smaller α than for $R_p = 1$ nm. Also, notice that the particle with $R_p = 1$ nm is now attracted for all wedge angles, unlike the previous case of $C = 3$ mM as in this case $\frac{U_p}{U_d} < 1$. For comparison, the magnitudes of the force acting on a particle at its closest position to the vertex for $K = 1$ and $\alpha = 45°$ is 1.2 , 1.6, and 0.22 pN for $R_p = 1$, 3, and 5 nm, respectively, where the first two forces are attractive and the last one is repulsive. For the best case scenario at 10 mM concentration ($K = 1$, $\alpha = 135°$, and $R_p = 3$ nm.), the ratio of particle densities is ∼1.6.

From the analysis of Eqs. (8) and (9) and contour plots of Fig. 2, one can see that in principle a charged particle can also experience an attractive force to the sidewall of the nanochannel. We can use the data in Figs. 4 and 5 to establish whether the particle is predominantly attracted to the vertex or to the wall of the nanochannel. To describe the interaction of a particle with the surface of a nanochannel away from the vertex, we can use the potentials for $\alpha = 180°$, i.e., the right most columns in Figs. 4 and 5. Direct comparison of the data between this column and data for the other angles α shows that attractive force is always stronger to the vertex than to the surface.

IV. CONCLUSION

In this work, we investigated how the nanochannel geometry and electrolyte concentration affect the electrostatic potential distribution and the charged particle behavior near the vertex of the nanochannel. For this purpose, we computed the electrostatic potential from the Poisson equation in the Debye approximation for a region near the corner of a nanochannel assuming a constant surface charge density on the nanochannel's surfaces. We also took into account the induced dielectrophoretic force, in order to see if it can be responsible for particle attraction to the vertex and/or side surfaces of a nanochannel.

We found that the greatest variation in the electrostatic potential occurs near the corners of a nanochannel. The wedge angle α, electrolyte concentration, values of Clausius-Mossotti factor, K, and particle size all affect particle behavior near the vertex. We found that the large particles and small ones exhibit attraction to the vertex only for certain electrolyte concentrations and wedge angles. However, particles of intermediate radius are attracted to the corner of a nanochannel for all four wedge angles α studied, irrespective of the electrolyte concentration, with $\alpha = 45°$, $K = 1$, and $C = 3$ mM being the case with the strongest attractive force between the particle and the vertex. We also studied how the electrolyte concentration affects the particle's attraction, and found that in order for large particles to get attracted to the vertex smaller concentrations of electrolyte need to be used. On the other hand, for small particles either larger concentrations of electrolyte or smaller wedge angles α are needed for this purpose.

From our results, we conclude that the dielectrophoresis can indeed overcome the Coulombic repulsion particularly for small wedge angles and small particle sizes. This could be the reason why DNA molecules are stretched along (attracted to) the corners of a nanochannel.

Appendix A: Details of the Numerical Integration

A freeware package, *bessk* [27, 28], was utilized to numerically calculate $K_{i\lambda}(x)$ in Eq. (3), $x = \kappa r$, for $0 < x \leq 20$ and $0 \leq \lambda \leq 400$. *bessk* can also output a scaled Bessel function, $K^S_{i\lambda}(x) = K_{i\lambda}(x)e^{\lambda\pi/2}$, which was also used in our numerical integration of $\Phi(r, \phi)$ for $400 \leq \lambda \leq 1500$.

In order to numerically evaluate the integral in Eq. (3), we used the trapezoidal method of integration with an integration step of 0.05. The integration was performed in the region of interest with a grid spacing of 0.08 nm in both x and y directions. For the integral in Eq. (3) to converge at points near the walls and away from the vertex, see Fig. 6, the upper limit of integration has to be set at $\lambda_{max} = 1500$.

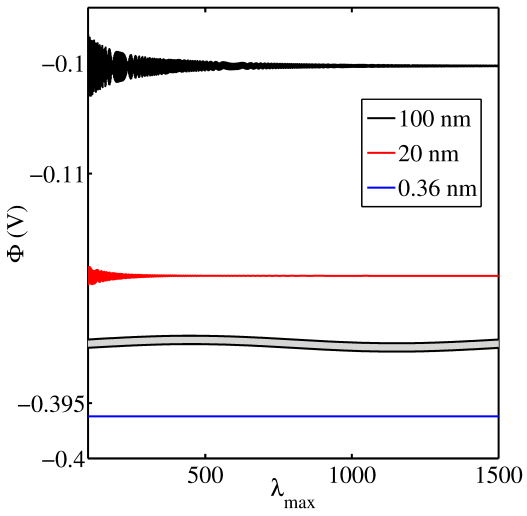

FIG. 6: (color online) Electrostatic potential Φ versus λ_{max} calculated at a distance of 0.16 nm from the bottom surface of the nanochannel, and at various distances from the vertex, 100 nm black (top) line, 20 nm red (middle) line, and 0.36 nm blue (bottom) line. The plot clearly shows that the farther away from the vertex, the larger the upper limit of integration λ_{max} is required to obtain an accurate value of the potential.

For this calculation the integral was split into three parts. In the first part, the direct integration of Eq. (3) was performed, but due to the machine specific limits

for evaluation of the exponentials, the range of λ was limited here to $0 < \lambda < 200$. For $200 < \lambda < 400$, approximations had to be made, so that the integration could be performed without invoking calculation of the scaled Bessel function. In this range, the integral in Eq. (3) was approximated without a loss of accuracy as

$$\int_{200}^{400} \frac{\sinh\left[\frac{\lambda\pi}{2}\right]}{\sinh[\lambda\alpha]} \left(\cosh[\lambda\phi] + \cosh[\lambda(\phi-\alpha)]\right) K_{i\lambda}(\kappa r) d\lambda = \frac{1}{2}\int_{200}^{400} e^{\lambda(\phi-\alpha)+\lambda\pi/2} K_{i\lambda}(\kappa r) d\lambda. \tag{A1}$$

For $400 < \lambda < 1500$, the scaled Bessel function was utilized in the integration, and in this range of λ's, Eq. (3) was approximated as

$$\int_{400}^{1500} \frac{\sinh\left[\frac{\lambda\pi}{2}\right]}{\sinh[\lambda\alpha]} \left(\cosh[\lambda\phi] + \cosh[\lambda(\phi-\alpha)]\right) K_{i\lambda}(\kappa r) d\lambda = \frac{1}{2}\int_{400}^{1500} \left(1 - e^{\lambda\pi}\right) e^{\lambda(\phi-\alpha)} e^{-\lambda\pi} K^S_{i\lambda}(\kappa r). \tag{A2}$$

Acknowledgments

This work was partially supported by the NSF grant DMR-1352218.

[1] M. Krishnan, I. Mönch, and P. Schwille, Nano Letters **7**, 1270 (2007).
[2] G. Salieb-Beugelaar, J. Teapal, J. van Nieuwkasteele, D. Wijnperlé, J. Tegenfeldt, F. Lisdat, A. van den Berg, and J. Eijkel, Nano Lett. **8**, 1785 (2008).
[3] A. Huang and A. Bhattacharya, EPL **106**, 18004.
[4] W. Yeo, K. Lee, Q. Guo, Y. Liu, X. You, J. Stamatoyannopoulos, and J. Chung, J. Nanotechnol. Eng. Med. **2**, 011004 (2011).
[5] M. Krishnan, Z. Petrek, I. Mönch, and P. Schwille, Small **4**, 1900 (2008).
[6] Y. Kim, K. S. Kim, K. L. Kounovsky, R. Chang, G. Y. Jung, J. J. dePablo, K. Jo, and D. C. Schwartz, Lab Chip **11**, 1721 (2011).
[7] D. R. Tree, Y. Wang, and K. D. Dorfman, Phys. Rev. Lett. **110**, 208103 (2013).
[8] P.-K. Lin, K.-h. Lin, C.-C. Fu, K.-C. Lee, P.-K. Wei, W.-W. Pai, P.-H. Tsao, Y.-L. Chen, and W. S. Fann, Macromolecules **42**, 1770 (2009).
[9] C.-C. Hsieh, A. Balducci, and P. S. Doyle, Nano Letters **8**, 1683 (2008).
[10] Y. Wang, D. R. Tree, and K. D. Dorfman, Macromolecules **44**, 6594 (2011).
[11] J. Regtmeier, T. T. Duong, R. Eichhorn, D. Anselmetti, and A. Ros, Anal. Chem. **79**, 3925 (2007).
[12] O. Castillo-Fernandez, G. B. Salieb-Beugelaar, J. W. van Nieuwkasteele, J. G. Bomer, M. Arundell, J. Samitier, A. van den Berg, and J. C. T. Eijkel, Electrophoresis **32**, 2402 (2011).
[13] J. D. Cross, E. A. Strychalski, and H. G. Craighead, J. Appl. Phys. **102**, 024701 (2007).
[14] L. D. Menard, C. E. Mair, M. E. Woodson, J. P. Alarie, and J. M. Ramsey, ACS Nano **6**, 9087 (2012).
[15] M. Tsutsui, M. Taniguchi, and T. Kawai, Nano Letters **9**, 1659 (2009).
[16] X. Liang and S. Y. Chou, Nano Letters **8**, 1472 (2008).
[17] S. H. Behrens and D. G. Grier, J. Chem. Phys. **115** (2001).
[18] K. H. Kang, I. S. Kang, and C. M. Lee, Langmuir **19**, 9334 (2003).
[19] W. B. Russel, W. R. Saville, and W. R. Schowalter, *Colloidal Dispersions* (Cambridge University Press, 1989) cambridge Books Online.
[20] M. I. Kontorovich and N. N. Lebedev, Zh. Eksp. Teor. Fiz. **8**, 1192 (1938).
[21] N. D. Fowkes and M. J. Hood, Q. J. Mech. Appl. Math. **51**, 553 (1998).
[22] M. Abramowitz, *Handbook of Mathematical Functions, With Formulas, Graphs, and Mathematical Tables,* (Dover Publications, Inc., 1974).
[23] J. D. Jackson, *Classical electrodynamics*, 3rd ed. (Wiley, New York, NY, 1999).
[24] M. Rasmusson and S. Wall, J. Colloid Interface Sci. **209**, 312 (1999).
[25] A. Nakano and A. Ros, Electrophoresis **34**, 1085 (2013).
[26] M. P. Hughes, Electrophoresis **23**, 2569 (2002).
[27] A. Gil, J. Segura, and N. M. Temme, ACM Trans. Math. Softw. **30**, 159 (2004).
[28] "Freeware package, *bessk*, available at http://dl.acm.org," .